HT2023-106015

MULTIMODAL CHARACTERIZATION OF STEADY-STATE AND TRANSIENT BOILING HEAT TRANSFER

Hari Pandey University of Arkansas Fayetteville, AR Christy Dunlap University of Arkansas Fayetteville, AR Amanda Williams University of Arkansas Fayetteville, AR Jackson Marsh University of Arkansas Fayetteville, AR

Han Hu University of Arkansas Fayetteville, AR

ABSTRACT

Boiling is a high-performance heat dissipation process that is central to electronics cooling and power generation. The past decades have witnessed significantly improved and bettercontrolled boiling heat transfer using structured surfaces, whereas the physical mechanisms that dominate structureenhanced boiling remain contested. **Experimental** characterization of boiling has been challenging due to the high dimensionality, stochasticity, and dynamicity of the boiling process. To tackle these issues, this paper presents a coupled multimodal sensing and data fusion platform to characterize boiling states and heat fluxes and identify the key transport parameters in different boiling stages. Pool boiling tests of water on multi-tier copper structures are performed under both steadystate and transient heat loads, during which multimodal, multidimensional signals are recorded, including temperature profiles, optical imaging, and acoustic signals via contact acoustic emission (AE) sensors, hydrophones immersed in the liquid pool, and condenser microphones outside the boiling chamber. The physics-based analysis is focused on i) extracting dynamic characteristics of boiling from time lags between acoustic-optical-thermal signals, ii) analyzing energy balance between thermal diffusion, bubble growth, and acoustic dissipation, and iii) decoupling the response signals for different physical processes, e.g., low-to-mid frequency range AE induced by thermal expansion of liquids and bubble ebullition. Separate multimodal sensing tests, namely a single-phase liquid test and a single-bubble-dynamics test, are performed to reinforce the analysis, which confirms an AE peak of 1.5 kHz corresponding to bubble ebullition. The data-driven analysis is focused on enabling the early fusion of acoustic and optical signals for

improved boiling state and flux predictions. Unlike single-modality analysis or commonly-used late fusion algorithms that concatenate processed signals in dense layers, the current work performs the fusion process in the deep feature domain using a multi-layer perceptron regression model. This early fusion algorithm is shown to lead to more accurate and robust predictions. The coupled multimodal sensing and data fusion platform is promising to enable reliable thermal monitoring and advance the understanding of dominant transport mechanisms during boiling.

Keywords: Boiling, Multimodal sensing, Data fusion, Acoustic emissions

NOMENCLATURE

AE	Acoustic Emission
CHF	Critical Heat Flux
EV	Electric Vehicles
DAQ	Data Acquisition
HTC	Heat Transfer Coefficient
pН	Potential of Hydrogen
Cu	Copper
FFT	Fast Fourier Transform
MLP	Multilayer Perceptron
PSD	Power Spectral Density
DNB	Departure from Nucleate Boiling

1. INTRODUCTION

Boiling occurs in various natural phenomena and several engineering applications such as fabric manufacturing [1],

nuclear power plants [2], water desalination [3], food and beverage industries [4], and hospitals and health care facilities [5]. For systems working involving phase change with high-temperature ranges, boiling is the dominant mode of heat transverse. Boiling introduces the phase change from liquid to a gaseous state. During the phase shift, a significant amount of heat is stored in latent form without any change in temperature rise [6]. Thus, boiling heat transfer is one of the effective cooling approaches for the thermal management process and extensive studies are invested in fully understanding this unpredictable and stochastic process.

The boiling process is accompanied by three distinct stages, namely natural convection from the boiling surface to the surrounding liquid, the bulk liquid convection infused by each bubble ebullition cycle, and vapor convection where direct heat is transferred from the heating surface to generating bubble. These three stages are depended on the thermal physical properties of working fluids, the morphological structure of the surface, bubble density, and departure diameter[7]. Higher bubble nucleation density at nucleate boiling regime promotes bulk convection which facilitates large heat removal. But, the neighboring bubbles have an affinity to coalesce together which can inhibit the removal of heat at high heat fluxes because of partial vapor covering the heating surface. This stage, called critical heat flux, is very detrimental to cooling and results in burnout of high-power density devices.

Based on thermal transport, boiling has been broadly classified into free convection, nucleate boiling, and transitional boiling stages which are followed by film boiling[8]. Nevertheless, an in-depth understanding of pool boiling from a different perspective such as acoustics, noise, optical, and power spectrum is not available. While several heat flux control strategies are put forward, the current pragmatic systems use the larger factor of safety in operation and run at relatively much lower heat fluxes. This is due to the erratic behavior of boiling and the lack of reliable techniques to monitor the system from a multi-modal approach. The existing system uses thermal monitoring which has accessibility issues and is also affected by the thermo-physical properties of the elements used within the compact system[9]. It is highly important to develop a multimodal approach relying on additional aspects with the thermal measurement to effectively predict and real-time monitoring of the boiling process. With that, a complete package of safety systems can be developed for a reliable, risk-free, and effective phase change cooling approach in near CHF situations while mitigating possible thermal mishaps.

Boiling is a very stochastic process and is sensitive to different experimental parameters including the thermo-physical properties of heating material and working fluid, surface wettability, pressure, pool temperature, heating orientation, gravity, and among others. Developing high-wetting surfaces[10]–[21] has been established as one of the promising methods for an advanced cooling approach which is supposed to constantly provide liquid delivery even at near-CHF heat fluxes and can attain the target for operating high power density systems at high temperatures. Although experimental

augmentation for boiling heat transfer has been extensively studied, the experimental characterization for different stages of pool boiling has yet to be fully understood. Moreover, a clear understanding of pool boiling behavior with adept prediction and control over CHF conditions is unavailable despite the extensive reach of boiling experiments and research.

A lab-scale boiling experiment with optical imaging comprises several large data sets extending from the temperature measurements, and pressure values to optical images for associated heat fluxes. Based on it, several optical images-based machine learning approaches[22]-[28] are used to characterize the boiling regimes which are highly dependent on in-house images and the working fluid's nature. This optical imagingbased control system cannot be fully used in real-case scenarios due to the necessity of a transparent boiling system and a similar working environment as the datasets. Thus, a new approach to characterizing the boiling process is essential which just not only is dependent on thermal or optical datasets of the boiling process. The multimodal characterization of the boiling process involves a large dataset with the motto of an in-depth understanding of pool boiling from different perspectives such as acoustics, noise/microphone, optical, and power spectrum. The availability of large datasets is very ideal for deep learning strategies where learning and recognizing the patterns is attainable and the predictions are based on multi-parameters that make the system more realistic.

Acoustic sensing is a non-intrusive, easy-to-implement system that has been used as an alternative for characterizing boiling research [29]. Different acoustic measurements like hydrophones, microphones, and acoustic sensors are used to identify the boiling regimes and associated heat fluxes for effective monitoring of the heating systems. The hydrophones are immersion in the liquid bath which detects the boiling anomaly based on differentiated sound signals. The microphones are remotely attached to the systems that record the change in noises that occurred due to increased heat fluxes. AE sensors sense the stress waves propagated within the systems when bolted on one of the edges and accurately predict the pre-CHF and CHF conditions with a noticeable spike in the different AE parameters including AE energy, AE count, and others. The existing acoustic approaches to boiling research are dominated by the frequency domain analysis and power spectral density over the sound signals obtained from the hydrophones or microphones. Despite the use of AE sensors in non-destructive testing, leakage detections, active corrosion, and crack propagation in avionics, among others, it has not been effectively used for the multi-modal prediction of boiling crisis.

Lim et al.[30] recorded the acoustic signal and established its correlation with the boiling regime and CHF. Alhashan et al. [31] investigated the early detection of bubble formation during boiling with acoustic emissions. It was found that AE parameters like AE-Energy, AE-Amplitude, and others are reliable, sensitive, and effective tools for monitoring the bubble process during the boiling phenomenon and identifying the overheating. Baek et al.[32] studied the acoustic emissions (AE) signals to monitor water boiling on fuel cladding surfaces. The boiling

behavior was monitored using AE signals and analyzed based on different AE parameters including hits, energy, and frequency. The relation between count and amplitude, two AE parameters, showed a consistent result with the boiling process. Seo et al. [33] studied the feasibility of boiling regimes identification based on AE features. Both the AE measurements and optical imaging was accompanied to differentiate between the boiling regimes with their associated characterized AE features.

In this work, we have performed multi-modal boiling characterization using temperature, optical images, and acoustic sensing (hydrophone, AE sensor, microphone) of two different heat load conditions in boiling heat transfer, that is steady-state and transient heat load conditions. This is because steady-state heat transfer has been extensively studied in literature but the actual real-time heat transfer is dominated by transient heat transfer whether it be in the battery management system of EVs or temperature control systems used in boilers of nuclear power plants. A detailed study showing the transient heat load is essential for ensuring the safety of systems working at larger heat fluxes. This is because the current cooling systems design is based on steady-state analysis that underpredicts the factor of safety. If an actual transient system is fully characterized and understood, the perfect monitoring of the cooling system can be imposed on high-power high-temperature applications which will save a lot of energy lost due to undervaluation.

2. MATERIALS AND METHODS

The project has two major aspects, that is, a) collection of synchronized data from transient and steady-state heat transfer conditions including all the optical images, acoustic emissions, microphone noises, and hydrophone signals as a function of time, and b) multi-modal characterization.

2.1 Experimental Setup

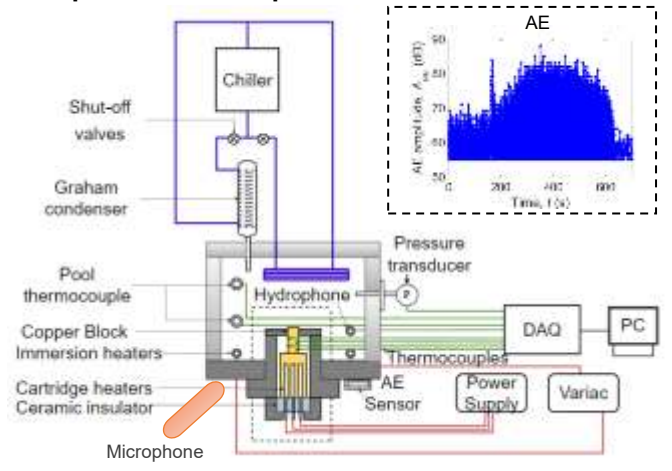


FIGURE 1: EXPERIMENTAL SETUP SHOWING BOILING CHAMBER WITH DIFFERENT SENSORS EMBEDDED WITHIN THE SYSTEM

Figure 1 shows the pool boiling experimental setup comprising the 1 cm² heating element of copper block inside the PEEK boiling chamber. A detailed description is provided in our

previous work [34]. For acoustic sensing, the acoustic sensor (MISTRAS R3a 30kHz) is attached to the outer edge of the boiling chamber to record the acoustic waves emitted during the pool boiling. During the AE measurement, a threshold frequency of 55 Hz is applied to the hardware acquisition software from Physical Acoustics Corporation (1283 USB AE Node) for reducing the possible background white noises over AE reading). A condenser microphone (Behringer ECM8000) connected to the main DAQ body (Behringer U-PHORIA UMC404HD) and powered by a 48V phantom power supply (Neewer NW-100) was used to measure noises generated outside of the boiling chamber. The DAQ can relay signals of 10Hz-43kHz and the microphone reads from 15Hz-20kHz. The DAQ is connected to the computer and the data is collected via LabVIEW.

2.2 Data Collection

The pool boiling data are collected over plain Cu surfaces as well as structured Cu foams-deposited boiling surfaces. For the pool boiling experiments, the multimodal signals were recorded from 0 to CHF conditions irrespective of the type of heat loading conditions. Also, the pool boiling experiments for each of the heat load types were done on four different samples, that is, polished copper, pH-0 deposited Cu foam, pH-10 deposited Cu foam, and pH-12 deposited Cu foam.

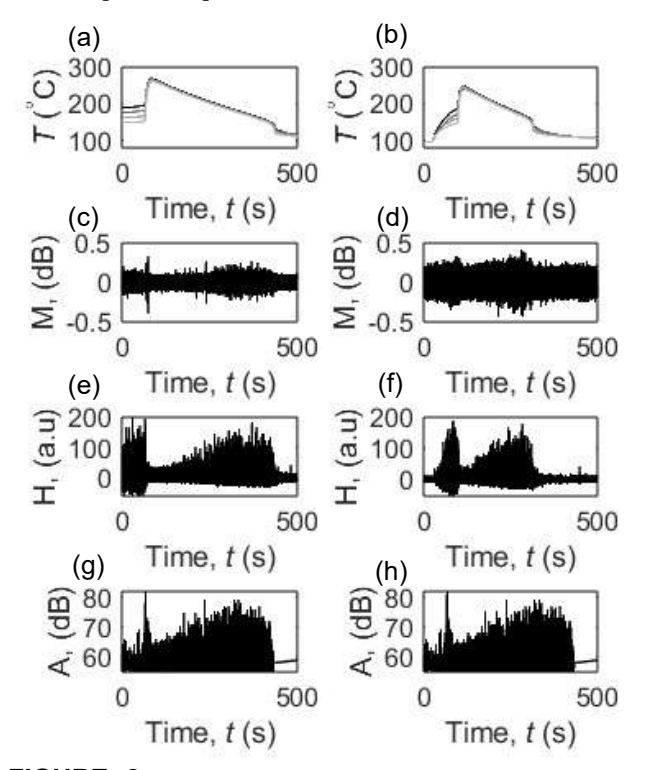


FIGURE 2: SYNCHRONIZED ACOUSTIC SIGNALS FOR STEADY STATE (A, C, E, G) AND TRANSIENT TESTING (B, D, F, G) RECORDED WITH THERMOCOUPLES (A, B), MICROPHONE (C, D), HYDROPHONE (E, F) AND AE SENSOR (G, H) OVER A PH-10 DEPOSITED CU FOAM SAMPLE

The datasets include multimodal signals such as optical images, acoustic signals (hydrophone, AE sensor), microphone

noises, and temperature profiles via thermocouples. The pool boiling setup as shown in **Figure 1** was used for collecting the data where two different sets of heat loading conditions were provided, that is, steady-state and transient heating. Steady-state heating observes the steady increase in the heat flux as a stepwise increment in the power of approximately 15 or 20 W until the CHF is triggered whereas, for transient heating, single ramp-up heating is applied till CHF occurred. All the datasets obtained are employed for the multi-modal analysis using machine learning algorithms.

The representative raw signals recorded from the different acoustic sensors, that is, AE sensor, microphone, and hydrophone respectively are shown in Figure 2. The tests are carried out both in a steady state followed by transient heat loading over the same pH-10 deposited Cu foam sample. CHF for the tests was reported to be 218.5634 W/cm² and 197.1744 W/cm² respectively. Figure 2a, b shows the temperature spike at the CHF. Following the trend, the acoustic waves in terms of AE amplitude recorded by the AE sensor also depict a large spike at the CHF point as shown in Figure 2g, h. Similarly, for the microphone and hydrophone data, their raw signals increase with the increased heat flux till CHF occurs. But, at the triggering of CHF, the raw signals get reduced as shown in Figure 2 c, d, e f respectively. The observed acoustic behavior during boiling is closely related to its physical phenomena. Boiling, a stochastic and unpredictable process, is much more complex and involves continuous bubble generation, bubble growth, and their departures from the hot surface inside the liquid pool. While doing so, it generates sound waves resulting in noise or vibrations. During the nucleate boiling, the acoustic thrust created by the bubble ebullition gradually increases with an increment in heat flux. But, at CHF, the boiling surface is blanketed by vapor film with exerts a significant sound pressure due to increased power density as shown in Figure 6,7,8 whether it be inside the liquid pool or on the boundary walls. The different acoustic devices pick up these waves and these AE signals can be used to investigate and understand boiling.

2.3 Multi-modal architecture

To show the potential of utilizing both high-speed image data and acoustic signals from a hydrophone together, three different machine-learning regression models were trained and

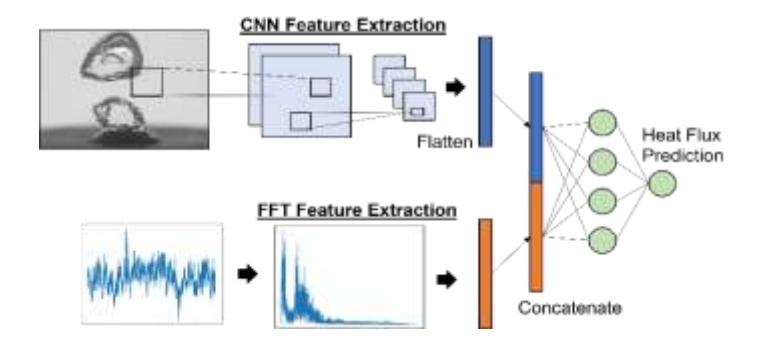


FIGURE 3: SCHEMATIC SHOWING THE ARCHITECTURE OF THE IMAGE AND ACOUSTIC FUSION MODEL.

tested for heat flux prediction. All of the models used data from the transient boiling test with the pH10 Cu foam. One model was a multilayer perceptron (MLP) and used segmented clips of the hydrophone signal converted to frequency intensities using the fast Fourier transform (FFT) to predict heat flux. Another model used only images reduced to 50 x 50 pixels from the pool boiling experiment. It coupled convolutional layers for feature extraction with an MLP for regression. The third model, which is shown in Figure 3, used both image data and acoustic signals. Feature extraction was performed on both data types (i.e. FFT for audio and convolutional layers for images) and was concatenated together and passed through an MLP for heat flux prediction. All three of the models used the same MLP structure for prediction. For the results of these models, the hydrophone signal was split into non-overlapping sequences of a length of 3000 samples. Each of the sequences was mapped to an image

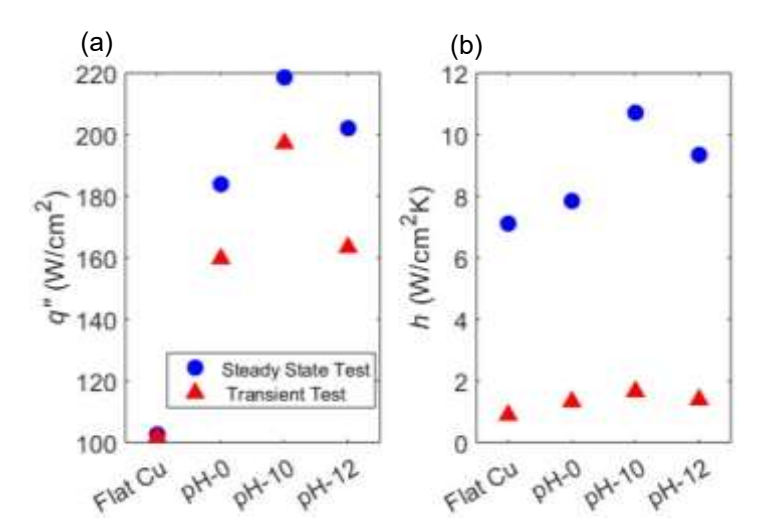


FIGURE 4: (A) CRITICAL HEAT FLUX AND (B) HEAT TRANSFER COEFFICIENTS FOR DIFFERENT BOILING SURFACES DURING STEADY STATE AND TRANSIENT HEAT LOAD CONDITIONS

and corresponding heat flux. For all the models, 80% of the data was used for training and 20% for testing. Each model was trained with the Adam optimizer and a mean squared error loss function. The FFT feature extraction was implemented using NumPy [35] and the models were implemented using TensorFlow [36].

3. RESULTS AND DISCUSSION

The respective pool boiling tests boiling parameters, which are, critical heat flux (CHF) and heat transfer coefficient (HTC) are plotted in **Figure 4**. The pH-10 Cu foam was found to have better performances in terms of CHF and HTC as compared to other Cu foams as well as flat polished copper surfaces. For the different modes of heat applications to the chamber, steady state condition has higher CHF and HTC values as compared to the transient testing.

3.1 Acoustic Analysis on Hydrophone signals

The acoustic signals recorded from the hydrophone, submerged inside the water bath, were further analyzed following the spectrogram. The acoustic frequency and energy obtained from spectrum analysis are used to characterize the acoustic waves. The spectrogram helps in determining the frequency as a function of time with the power intensity at each time frame.

3.1.1 Acoustic Features of Single Bubble Dynamics

The key optical, acoustic, and thermal characteristics of bubble nucleation and release are recorded and analyzed for individual air bubbles. These characteristics, including frequency, period, amplitude, etc. will set a reference for the analysis of multi-bubble dynamics. Figure 5 shows the schematic drawing for the air bubble system and test results. Air bubbles are generated and released using a programmable syringe pump. The bubble dynamics are visualized using VIS high-speed imaging. Acoustic signals are measured using a hydrophone immersed in the liquid pool and an AE sensor attached to the bottom of the pool. The bubble trajectories are analyzed using high-speed videos with results presented in figure 5b. The rising velocity of the small bubble is 150 mm/s, lower than that of the large bubble (177 mm/s). As shown in figure 5c, the spectrograms from the hydrophone signals show spikes at the moment of the bubble rising. The peak frequency of the 3.94 mm bubble is approximately 1.45 kHz, which is consistent with the natural frequency of Minnaert resonance calculated to be 1.432 kHz following $f = (2\pi r)^{-1} (3\gamma P/\rho_1)^{0.5}$, where r is the bubble radius, γ polytropic coefficient, P pressure, and ρ_1 liquid density.

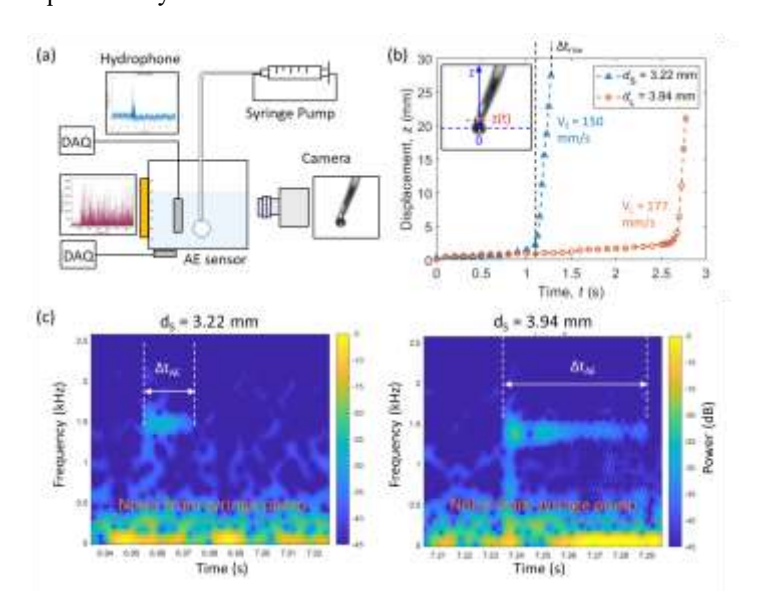


FIGURE 5: OPTICAL AND ACOUSTIC FEATURES OF SINGLE AIR BUBBLE DYNAMICS SHOWING (A) SCHEMATIC DRAWING OF THE TEST FACILITY OF AIR BUBBLE DYNAMICS CHARACTERIZATION, (B) TRAJECTORIES OF BUBBLES FROM HIGH-SPEED IMAGING, AND (C) SPECTROGRAMS OF AIR BUBBLE TESTS USING DIFFERENT TUBE DIAMETERS.

3.1.2 Acoustic Features of Pool Boiling Bubble Dynamics

Both the steady state and transient testing spectral analysis is analyzed below:

3.1.2.1 Steady State Boiling Spectral Analysis

Spectral analysis for the hydrophone signals recorded during the boiling experiment over pH-10 Cu foams is shown in Figure 6. At the CHF initiation, both the frequency and heat flux is observed to reduce significantly implying the heat transfer insulation caused by vapor wrapping on the boiling surface. As the spectrogram is analyzed, a common trend can be observed between the heat flux and maximum power spectral density. Both of them keep on increasing at the step heat supply increment but once CHF occurs, values of both parameters have plummeted. Moreover, the frequency at maximum PSD is shifted towards a higher frequency range at the CHF state as shown in Figure 6d.

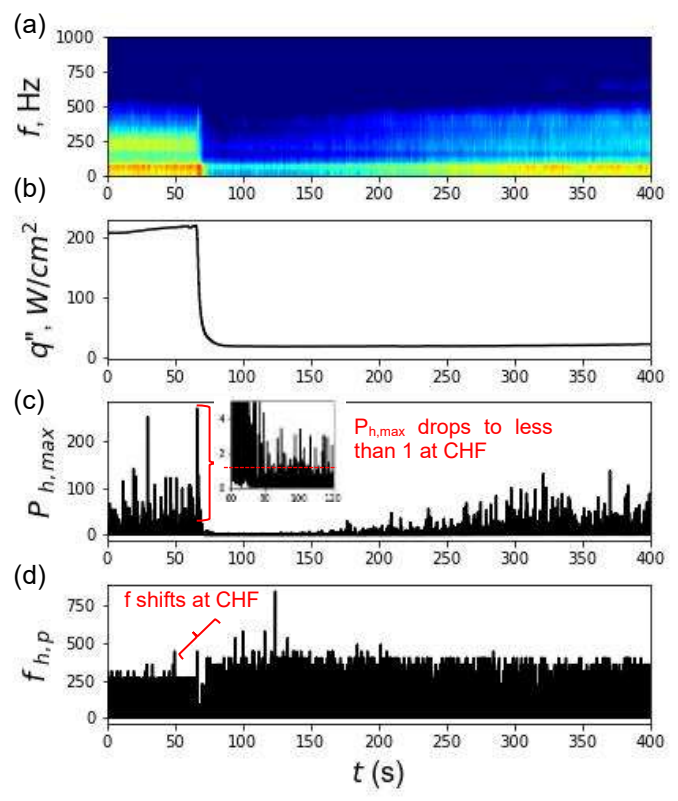


FIGURE 6: SPECTRAL ANALYSIS FOR THE CRITICAL HEAT FLUX CONDITION OF A STEADY-STATE TEST SHOWING SYNCHRONIZED (A) SPECTROGRAM, (B) HEAT FLUX, (C) MAXIMUM POWER, AND (D) DOMINANT FREQUENCY OVER TIME.

Figure 7 shows the power spectral density during steady-state boiling on different boiling surfaces. The steady-state test results show an increased power level with heat flux in the nucleate boiling regime. But when CHF is triggered, the acoustic power is reduced by more than 2 orders of magnitude within 0.0112 seconds. Since the acoustic power scales with the square of its

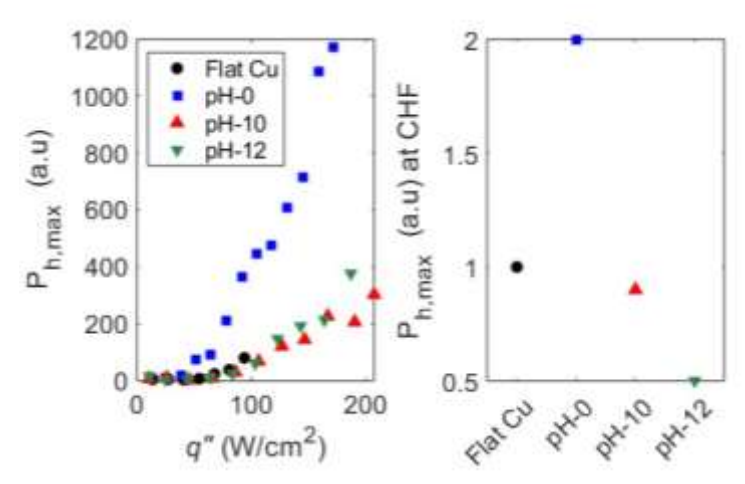


FIGURE 7: POWER SPECTRAL DENSITY FOR THE STEADYSTATE BOILING OVER PH-10 SAMPLE VERSUS HEAT FLUX.

frequency, energy frequency via acoustic waves significantly decreases.

3.1.2.2 Transient Boiling Raw Data Spectral Analysis

For transient testing, a ramp-up heat is provided from 0 to CHF condition in one go. Three different stages are observed including nucleate boiling to pre-CHF, pre-CHF to transition boiling i.e. DNB (departure from nucleate boiling), and DNB to NB as the heat supply is turned off. Figure 8 represents the spectral analysis for the transient test conducted over a pH-10 deposited Cu sample. From the spectral analysis, it can be noted that the frequency, heat flux, and PSD max are increasing with the increased applied heat load. But at the CHF point, all of these three parameters are decreased significantly. Moreover, the frequency at PSD max is reduced at the CHF point and will stay the same until the boiling reversal occurs where the departure from the nucleate boiling state is reversed back to the nucleate boiling regime. At this state, the frequency at maximum PSD is shifted from low to high and resembles back to the frequencies present at the initial stages of the boiling process at the nucleate boiling regime. This shows that there is a characteristic frequency in the NB regime and transition boiling regime. Such understanding can be leveraged in CHF detection and monitoring systems based on either frequency shift recognition or PSD max differential values as the function of the temporal axis.

3.2 AE sensor amplitude analysis for pool boiling

The acoustic sensing in terms of amplitude is recorded using AE sensors attached to the bottom of the boiling chamber. The AE amplitude, defined by Physical Acoustics, is plotted for the different boiling surfaces at CHF as shown in **Figure 9**. It can be concluded that irrespective of the heat loading type the acoustics waves detected by the AE sensor were very close to each other. But, at the CHF triggering there is a significant spike in AE amplitude as shown in **Figure 2g**, h which differentiates the

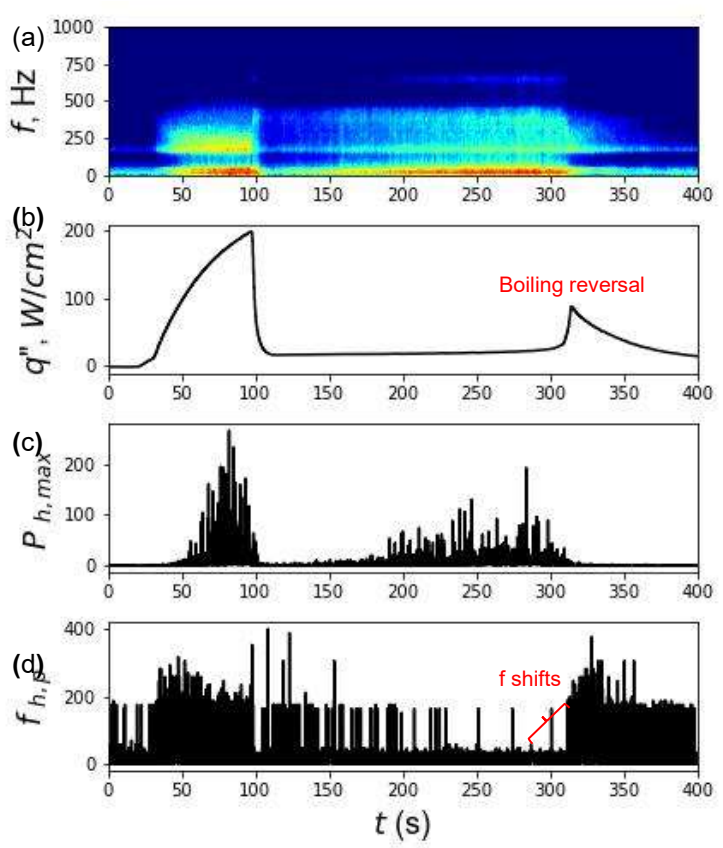


FIGURE 8: SPECTRAL ANALYSIS FOR A TRANSIENT POOL BOILING TEST SHOWING SYNCHRONIZED (A) SPECTROGRAM, (B) HEAT FLUX, (C) MAXIMUM POWER, AND (D) DOMINANT FREQUENCY OVER TIME.

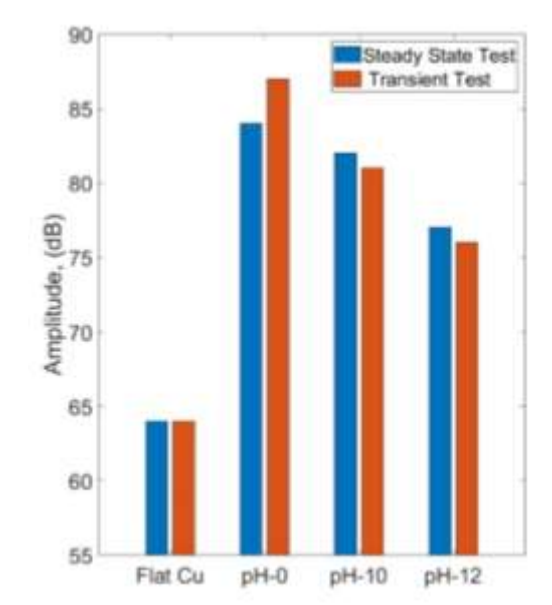


FIGURE 9: AE AMPLITUDE RECORDED AT CHF FOR STEADY-STATE AND TRANSIENT TESTING RESPECTIVELY

transition boiling initiation from the nucleate boiling regime. AE amplitude threshold value of 55 dB was provided to mitigate the background white signals, present if any during the experiments. As such the AE amplitude can be seen with values larger than 55 dB. A common trend of slightly higher AE amplitude is observed for the steady-state test as compared to the transient test with pH-0 being an exception. For the pH-0 case, the amplitude for the transient test is larger than the steady state one.

3.3 Image-based vapor fraction analysis for boiling tests

The vapor flux analysis is performed on the boiling images to understand the bubble dynamics in both the steady state and transient heating conditions. As shown in **figure 10**, the vapor generation is increased with the increased heat flux in the transient heating case. But, at the CHF initiation, the vapor flux is reduced tremendously indicating the stubby bubble blanketing on the boiling surface. A proper real-time vapor contour analysis can be used to correlate with boiling stages and potentially identify the CHF initiation.

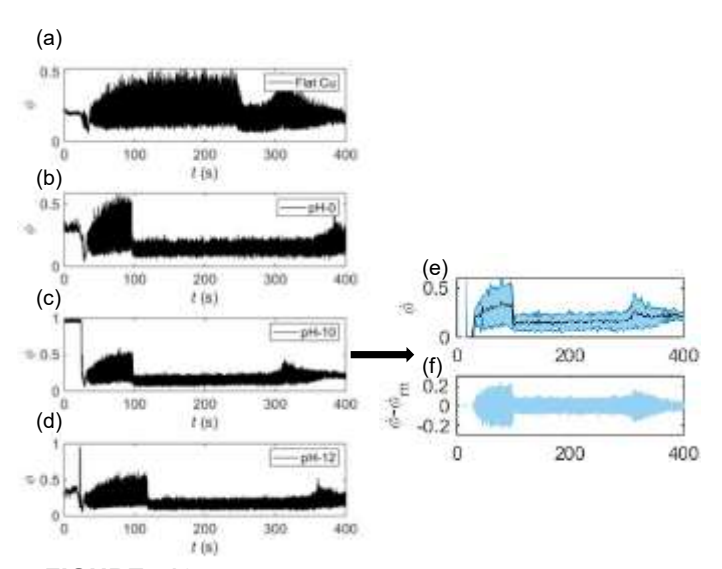


FIGURE 10: VAPOR FRACTION ANALYSIS FOR A TRANSIENT TESTING DONE ON DIFFERENT BOILING SURFACES (A, B, C, D) WHERE A TRANSIENT TEST (C) IS FURTHER ANALYZED WITH MEAN VAPOR FRACTION SHOWING THE INCREASE IN VAPOR AS A FUNCTION OF TIME WITH INCREASED HEAT FLUX

The different steady-state boiling experiments conducted on various boiling surfaces and their mean vapor fraction vs the heat flux is shown in **Figure 11**. **Figures 10** and **11** show a common trend that irrespective of heat load conditions the mean vapor fraction is increased with the increased heat flux. This behavior is observed till the CHF triggering occurs.

3.4 Multimodal Fusion

Both the acoustic (from hydrophone) and optical data were combined to predict the heat flux. After training all three regression models, the coefficient of determination (R^2 score) results are shown in **Figure 12**.

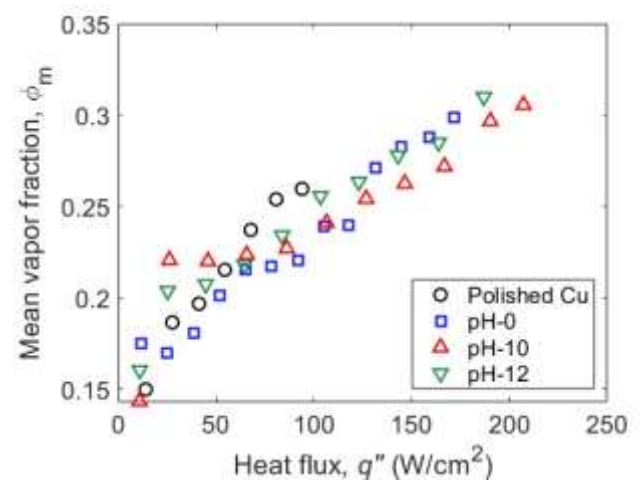


FIGURE 11: VAPOR FRACTION FOR STEADY-STATE HEAT LOAD CONDITION

The R² score is a measurement of the fit of the model to the data. Values close to 1 are desired and indicate a good fit. The image regression model performed the worst with an R² score of 0.68. This could be due to the reduced image size and small training set. The fusion model did the best with an R² score of 0.941 but just slightly better than the sound model with an R² score of 0.928. This is also seen in **Figure 13** where the predicted values of heat flux vs the true heat flux labels are plotted for all three models. Ideally, the points would all lie on the diagonal line implying the predicted heat flux is the same as the true heat flux label. It can be seen here that the fusion model and sound model do the best. From these results, it is shown that there is promise in improving the accuracy by incorporating both image data and sound data in a fusion model.

This can be attributed to different approaches, whether it be optical or acoustic data acquisition, implemented in the very

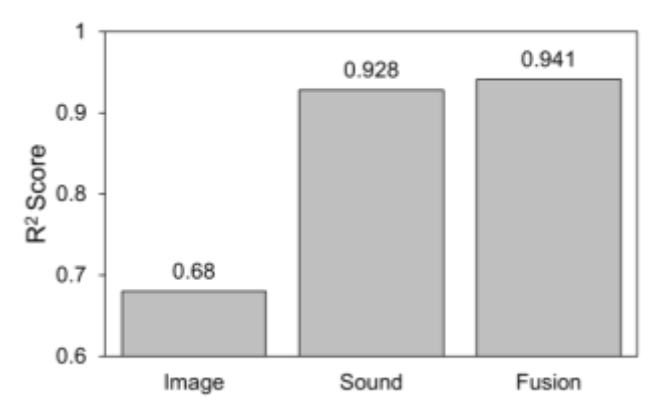


FIGURE 12: R² SCORES FOR ALL THREE MODELS; IMAGE CNN-MLP, SOUND FFT-MLP, AND IMAGE-SOUND FUSION MODEL.

same boiling process. The method for procuring the images and sounds would be independent of themselves but they are

corresponding to the same physical phenomenon. As a result, a fusion of both optic-acoustic models can be anticipated complimenting each other which shows great promise in the effective prediction of heat fluxes.

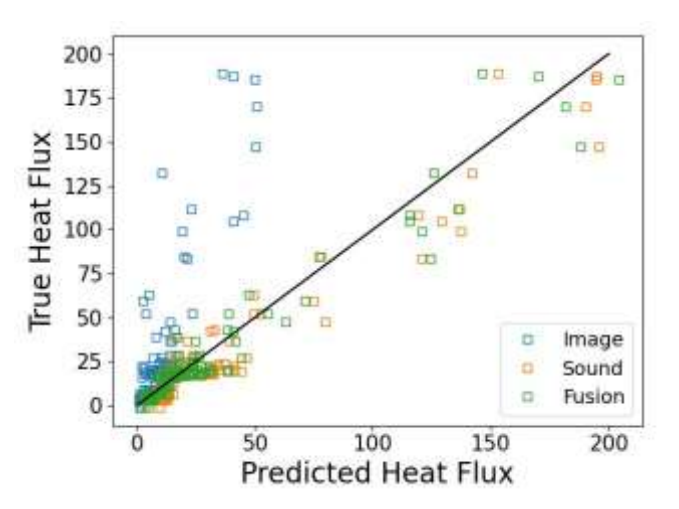


FIGURE 13: TRUE HEAT FLUX LABEL VS PREDICTED HEAT FLUX LABEL FOR ALL THREE MODELS; IMAGE-ONLY MODEL, SOUND-ONLY MODEL, AND IMAGE-SOUND FUSION MODEL.

3.5 Limitations of the study

This boiling study was performed over the electrodeposited copper foams and polished copper surfaces at different heat load conditions. While doing so, the current study was susceptible to several limitations that could be grouped into two major categories: a. Data collection limitations b. Machine learning fusion limitations. Some of those limitations and future directions for mitigating such issues are discussed below:

3.5.1 Data collection limitations

- During both the SteadyState and Transient boiling experiments, the boiling setup was exposed to the surrounding noises. This study implements the threshold values for AE sensors to diminish the white noises but the data from the microphone and hydrophones are adulterated by the noises. For minimizing this effect, the complete setup was kept in a low-noise environment. For future approaches, noise reduction filters can be implemented over hydrophone
- 2. In each pool boiling experiment, two hydrophones were placed inside the saturated water bath and tried to be fixed at a position. As boiling is such a vigorous process, the vehement bubble generation induced the vibration over the hydrophones. Also, the geometrical location, its position from the heating area as well as orientation could alter the sound signal recording. For averaging out these odds, we used two different hydrophones in alternate directions. These differences in data could potentially reduce the aforementioned issues with hydrophones' location.
- 3. Deionized water is used as the thermal transport media

during the boiling tests. The acoustic characteristics could vary depending on the liquid properties such as viscosity, boiling point, etc. which are not explored in this study.

3.5.2 Machine learning limitations

The acoustic and fusion machine learning models presented in the paper are shown to have high performance in the testing phase. However, the performance of these models may be limited when faced with more diverse testing data. For example, changing the copper surface or the boiling fluid could significantly affect the model's performance. Moreover, the use of acoustics as a sensor makes the model sensitive to background noise, which could also impact the results. To overcome these limitations, various approaches have been developed, such as incorporating more diverse data during training, utilizing domain adaption techniques, and using transfer learning with pre-trained models fine-tuned on additional data. By implementing these strategies, the performance of the machine learning models can be more generalized and improved, ultimately leading to better results.

4. CONCLUSION

The multi-model characterization of two different heating applications including steady state and transient is done in this paper with a focus on early prediction and effective monitoring of boiling crisis. The acoustics signals obtained from different sensors such as hydrophone, and AE sensors show a definite change during the CHF initiation whether it be the dominant acoustic frequency and power level of hydrophone signals or the amplitude recorded for the AE sensor. A single bubble analysis is done to understand the bubble footprints from spectrogram analysis and it is further applied to the pool boiling. The vapor flux analysis depicted the increment in vapor fraction as the heat flux increased and was seen to decrease dramatically at the CHF point. Finally, three different machine-learning regression models were tested for understanding the potential fusion implementing both the high-speed images and acoustic signals in an attempt to characterize boiling processes. Future work will focus on incorporating a variety of boiling environments and potentially develop a generalized non-intrusive fault detection model for high-performance cooling environments involving boiling.

ACKNOWLEDGEMENTS

This study was supported by the National Science Foundation under Grant No. TI-2212002, the Arkansas Space Grant Consortium under Arkansas NASA EPSCoR RID 242043-23UAF.Hu, and the University of Arkansas through the Chancellor's Commercialization Fund and GAP Fund. A.W. appreciates the support from the Arkansas Space Grant Consortium STEM Program. J.M. appreciates the support from the Arkansas Space Grant Consortium Student Intensive Training Program and the University of Arkansas Honors College Research Grant.

REFERENCES

- [1] S. S. Patil, A. K. Bewoor, and R. B. Patil, "Availability analysis of a steam boiler in textile process industries using failure and repair data: A case study," *ASCE-ASME Journal of Risk and Uncertainty in Engineering Systems, Part B: Mechanical Engineering*, vol. 7, no. 2, 2021, doi: 10.1115/1.4049007.
- [2] S. Evens, "A complicated way of boiling water: nuclear safety in water history," *Water Hist*, vol. 12, no. 3, pp. 331–344, 2020, doi: 10.1007/s12685-020-00258-0.
- [3] M. Shatat and S. B. Riffat, "Water desalination technologies utilizing conventional and renewable energy sources," *International Journal of Low-Carbon Technologies*, vol. 9, no. 1, pp. 1–19, 2014, doi: 10.1093/ijlct/cts025.
- [4] A. M. Salamatullah *et al.*, "Boiling technique-based food processing effects on the bioactive and antimicrobial properties of basil and rosemary," *Molecules*, vol. 26, no. 23, 2021, doi: 10.3390/molecules26237373.
- [5] J. H. Yoo, "Review of disinfection and sterilization Back to the basics," *Infect Chemother*, vol. 50, no. 2, pp. 101–109, 2018, doi: 10.3947/ic.2018.50.2.101.
- [6] V. P. Carey, Liquid-Vapor Phase-Change Phenomena. CRC Press, 2020. doi: 10.1201/9780429082221.
- [7] CHI-YEH HAN PETER GRIFFITH, "THE MECHANISM OF HEAT TRANSFER IN NUCLEATE POOL BOILING CHI-YEH HAN Report No . 7673-19 Department of Mechanical Engineering Massachusetts Institute of Technology," *Engineering*, 1962.
- [8] B. Liščić, S. Singer, and M. Processing, "Nucleate Boiling Thermal Engineering of Steel Alloy Sys- tems," 2019.
- [9] I. Atomic *et al.*, "Monitoring and Diagnosis Systems to Improve Nuclear Power Plant Reliability and Safety," no. May, 1996.
- [10] H. S. Ahn, C. Lee, J. Kim, and M. H. Kim, "The effect of capillary wicking action of micro/nano structures on pool boiling critical heat flux," *Int J Heat Mass Transf*, vol. 55, no. 1–3, pp. 89–92, Jan. 2012, doi: 10.1016/j.ijheatmasstransfer.2011.08.044.
- [11] A. Rokoni, D.-O. Kim, and Y. Sun, "Micropattern-controlled wicking enhancement in hierarchical micro/nanostructures," *Soft Matter*, vol. 15, no. 32, pp. 6518–6529, Aug. 2019, doi: 10.1039/C9SM01055F.
- [12] H. Hu, J. A. Weibel, and S. V. Garimella, "A coupled wicking and evaporation model for prediction of pool boiling critical heat flux on structured surfaces," *Int J Heat Mass Transf*, vol. 136, pp. 373–382, 2019, doi: 10.1016/j.ijheatmasstransfer.2019.03.005.
- [13] M. M. Rahman, S. Ridwan, D. Fehlinger, and M. Mccarthy, "Wicking Enhanced Critical Heat Flux for Highly Wetting Fluids on Structured Surfaces," *Langmuir*, vol. 36, no. 32, pp. 9643–9648, 2020, doi: 10.1021/acs.langmuir.9b03711.

- [14] B. S. Kim, H. Lee, S. Shin, G. Choi, and H. H. Cho, "Interfacial wicking dynamics and its impact on critical heat flux of boiling heat transfer," *Appl Phys Lett*, vol. 105, no. 19, p. 191601, Nov. 2014, doi: 10.1063/1.4901569.
- [15] J. Li, W. Fu, B. Zhang, G. Zhu, and N. Miljkovic, "Ultrascalable Three-Tier Hierarchical Nanoengineered Surfaces for Optimized Boiling," *ACS Nano*, vol. 13, no. 12, pp. 14080–14093, 2019, doi: 10.1021/acsnano.9b06501.
- [16] A. Mirza Gheitaghy, H. Saffari, and G. Qi Zhang, "Effect of Nanostructured Microporous Surfaces on Pool Boiling Augmentation," 2018, doi: 10.1080/01457632.2018.1442310.
- [17] D. F. Hanks *et al.*, "Nanoporous membrane device for ultra high heat flux thermal management," *Microsyst Nanoeng*, vol. 4, no. 1, pp. 1–10, 2018, doi: 10.1038/s41378-018-0004-7.
- [18] A. R. Betz, J. Xu, H. Qiu, and D. Attinger, "Do surfaces with mixed hydrophilic and hydrophobic areas enhance pool boiling?," *Appl Phys Lett*, vol. 97, no. 14, pp. 14–16, 2010, doi: 10.1063/1.3485057.
- [19] M. Bongarala, H. Hu, J. A. Weibel, and S. v Garimella, "Microlayer evaporation governs heat transfer enhancement during pool boiling from microstructured surfaces Microlayer evaporation governs heat transfer enhancement during pool boiling from microstructured surfaces," *Appl Phys Lett*, vol. 221602, no. May, 2022, doi: 10.1063/5.0090156.
- [20] M. Bongarala, H. Hu, J. A. Weibel, and S. v. Garimella, "A figure of merit to characterize the efficacy of evaporation from porous microstructured surfaces," *Int J Heat Mass Transf*, vol. 182, 2021, doi: 10.1016/j.ijheatmasstransfer.2021.121964.
- [21] H. Hu, J. A. Weibel, and S. v. Garimella, "A coupled wicking and evaporation model for prediction of pool boiling critical heat flux on structured surfaces," *Int J Heat Mass Transf*, vol. 136, pp. 373–382, 2019, doi: 10.1016/j.ijheatmasstransfer.2019.03.005.
- [22] S. Moein Rassoulinejad-Mousavi *et al.*, "Deep learning strategies for critical heat flux detection in pool boiling," 2021, doi: 10.1016/j.applthermaleng.2021.116849.
- [23] Y. Suh, R. Bostanabad, and Y. Won, "Deep learning predicts boiling heat transfer," *Sci Rep*, vol. 11, p. 5622, 123AD, doi: 10.1038/s41598-021-85150-4.
- [24] K. N. R. Sinha, V. Kumar, N. Kumar, A. Thakur, and R. Raj, "Deep learning the sound of boiling for advance prediction of boiling crisis," *Cell Rep Phys Sci*, vol. 2, no. 3, p. 100382, 2021, doi: 10.1016/j.xcrp.2021.100382.
- [25] G. M. Hobold and A. K. da Silva, "Machine learning classification of boiling regimes with low speed, direct and indirect visualization," *Int J Heat Mass Transf*, vol. 125, pp. 1296–1309, 2018, doi: 10.1016/j.ijheatmasstransfer.2018.04.156.

- [26] F. Al-Hindawi *et al.*, "A Generalized Framework for Critical Heat Flux Detection Using Unsupervised Image-to-Image Translation," vol. 1, no. 602, 2022, [Online]. Available: http://arxiv.org/abs/2212.09107
- [27] C. Dunlap, H. Pandey, and H. Hu, "Supervised and Unsupervised Learning Models for Detection of Critical Heat Flux during Pool Boiling," in *Proceedings of the ASME 2022 Heat Transfer Summer Conference*, 2022.
- [28] A. Rokoni, L. Zhang, T. Soori, H. Hu, T. Wu, and Y. Sun, "Learning new physical descriptors from reduced-order analysis of bubble dynamics in boiling heat transfer," *Int J Heat Mass Transf*, vol. 186, p. 122501, 2022, doi: 10.1016/j.ijheatmasstransfer.2021.122501.
- [29] H. Hu, H. Pandey, and C. Dunlap, "Detecting or Predicting System Faults in Cooling Systems in a Non-Intrusive Manner Using Deep Learning," 2022
- [30] D. Y. Lim, S. B. Seo, K. M. Kim, I. C. Bang, and U. States, "A Detection of Acoustic Emission Signals from the Pool Boiling Condition for Determining Boiling Phenomena," pp. 24–26, 2019.
- [31] T. Alhashan, A. Addali, J. Amaral Teixeira, and S. Elhashan, "Identifying bubble occurrence during pool boiling employing acoustic emission technique," *Applied Acoustics*, vol. 132, no. October 2017, pp. 191–201, 2018, doi: 10.1016/j.apacoust.2017.11.006.
- [32] S. H. Baek, K. Wu, H. S. Shim, D. H. Lee, J. G. Kim, and D. H. Hur, "Acoustic emission monitoring of water boiling on fuel cladding surface at 1 bar and 130 bar," *Measurement (Lond)*, vol. 109, pp. 18–26, 2017, doi: 10.1016/j.measurement.2017.05.042.
- [33] S. Bin Seo and I. C. Bang, "Acoustic analysis on the dynamic motion of vapor-liquid interface for the identification of boiling regime and critical heat flux," *Int J Heat Mass Transf*, vol. 131, pp. 1138–1146, 2019, doi: 10.1016/j.ijheatmasstransfer.2018.11.136.
- [34] H. Pandey, W. Waldo, and H. Hu, "Non-Intrusive Cooling System Fault Detection and Diagnostics Using Acoustic Emission," 2022, vol. ASME 2022 Heat Transfer Summer Conference. doi: 10.1115/HT2022-85429.
- [35] C. R. Harris *et al.*, "Array programming with NumPy," *Nature*, vol. 585, no. 7825, pp. 357–362, 2020, doi: 10.1038/s41586-020-2649-2.
- [36] M. Abadi et al., "TensorFlow: A system for large-scale machine learning," Proceedings of the 12th USENIX Symposium on Operating Systems Design and Implementation, OSDI 2016, pp. 265–283, 2016.